

# An adaptive watermarking for remote sensing images based on maximum entropy and discrete wavelet transformation

Yang Hua<sup>1</sup>, Xu Xi<sup>1\*</sup>, Chengyi Qu<sup>1</sup>, Jinglong Du<sup>1\*</sup>, Maofeng Weng<sup>2</sup>, and Bao Ye<sup>3</sup>

<sup>1</sup> School of Geography Science and Geomatics Engineering, Suzhou University of Science and Technology, Suzhou 215000 China

[e-mail: xixu@usts.edu.cn]

<sup>2</sup> Northwest Engineering Corporation Limited, PowerChina, Xi'an 710065 China

<sup>3</sup> Suzhou Industrial Park Surveying Mapping and Geoinformation Co. Ltd, Suzhou 215000 China

\*Corresponding author: Xu Xi, Jinglong Du

*Received August 8, 2023; revised October 14, 2023; accepted January 1, 2024;  
published January 31, 2024*

---

## Abstract

Most frequency-domain remote sensing image watermarking algorithms embed watermarks at random locations, which have negative impact on the watermark invisibility. In this study, we propose an adaptive watermarking scheme for remote sensing images that considers the information complexity to select where to embed watermarks to improve watermark invisibility without affecting algorithm robustness. The scheme converts remote sensing images from RGB to YCbCr color space, performs two-level DWT on luminance  $Y$ , and selects the high frequency coefficient of the low frequency component ( $HH_2^Y$ ) as the watermark embedding domain. To achieve adaptive embedding,  $HH_2^Y$  is divided into several  $8*8$  blocks, the entropy of each sub-block is calculated, and the block with the maximum entropy is chosen as the watermark embedding location. During embedding phase, the watermark image is also decomposed by two-level DWT, and the resulting high frequency coefficient ( $HH_2^W$ ) is then embedded into the block with maximum entropy using  $\alpha$ -blending. The experimental results show that the watermarked remote sensing images have high fidelity, indicating good invisibility. Under varying degrees of geometric, cropping, filtering, and noise attacks, the proposed watermarking can always extract high identifiable watermark images. Moreover, it is extremely stable and impervious to attack intensity interference.

---

**Keywords:** remote sensing image; watermark; YCbCr; DWT; adaptive

---

This work was supported by the National Natural Science Foundation of China (42101420) and Suzhou Industrial Prospects and Key Core Technology Projects (SYC2022028).

## 1. Introduction

As an essential national fundamental strategic information resource, remote sensing images play an important role in urban planning, military applications, catastrophe prevention and forecast, agricultural production, etc., which has a substantial socioeconomic value [1-3]. As advancements continue to be made in the fields of space exploration, sensor technology, and computer science, the amount of remote sensing images is rapidly growing, data resolution is getting higher and higher, and demand for remote sensing images in social development is also increasing [4, 5].

Currently, developed network platforms and portable hardware facilitate the transmission and sharing of remote sensing images, helping them to be quickly integrated into social services; nevertheless, they also pose serious data security problems. Theft, copying, selling, and tampering of remote sensing images are becoming more and more frequent due to their extremely comprehensive geographic information and high value, thereby affecting the interests of data producers and legitimate owners, and even threatening national and territorial security [6-8]. Digital watermarking, as a cutting-edge technology in the realms of information security and copyright protection, is attracting more attention and has been widely applied to remote sensing images. Since the proposal of digital watermarking technology, both academia and industry have devoted significant resources to the research and development of this technology, and there are already many mature watermarking technologies and products that are widely used to protect the security of various types of electronic data [9-12]. According to the embedding method of the watermark, watermarking of remote sensing images can be categorized into two types: spatial-domain and frequency-domain watermarking [13]. In most cases, remote sensing images are watermarked in the spatial domain by directly altering their pixel value, gray value, or brightness value. By altering the pixel values of remote sensing images, Kumari et al. [14] introduced watermark information and then utilized the difference between the two to verify proper watermark embedding. Zhu et al. [15] processed the segmentation and encryption of remote sensing images and embedded watermarks into the pixel values by additional rules. This method has excellent invisibility, however, it is not a blind watermarking. Khosravi et al. [16] further improved the algorithm by replacing the additive rule of watermark embedding with the rule of inter-pixel relationship judgment, thus achieving blind extraction. Ren et al. [17] spread the original watermark information, matched the watermark value with the highest valid bit of the pixel value of the remote sensing image to generate a key matrix, and embedded the watermark into the highest bit or the next lowest bit through the LSB method. The spatial-domain watermarking technique is straightforward to deploy and causes little to no disruption to the original data. However, the algorithm is susceptible to pixel value changes and has low robustness in general, limiting its practicality [13, 18].

Algorithms for embedding watermarks in images using the frequency domain do so by transforming images from the spatial domain to the frequency domain and then altering the frequency coefficients. Discrete Fourier transform (DFT), discrete wavelet transform (DWT), and discrete cosine transform (DCT) are typical frequency domain transform techniques [13, 19]. Tong et al. [20] used compressed sensing to pre-process the watermark information by dividing the remote sensing image into robust and variable domains using DWT and embedding the watermark information into the variable domain through a mapping mechanism, which is robust to cropping and noise attacks. Yuan et al. [21] applied a three-dimensional DWT to the divided remote sensing images and embedded watermark information by means of a coefficient quantization. The method's resilience was all-encompassing, standing up well

to geometric attacks and noise attacks, etc. Li et al. [22] performed pretreatment normalization on remote sensing images, selected an invariant region for DFT, split the watermark into two parts, and embedded these two parts in the phase and magnitude of the DFT, respectively. This method is resistant to compression and geometric attacks. Li et al. [23] used the quaternion wavelet transform (QWT) to transform the remote sensing images. The most stable coefficients were then filtered as the watermark embedding domain by tensor decomposition. Compared with conventional DWT or QWT watermarking algorithms, this technique is more comprehensive and robust. Qin et al. [24] employed the ASIFT algorithm to extract feature points of remote sensing images and to generate feature regions. After applying two-dimensional DWT to the feature regions, watermark information was embedded in the low frequency coefficients. This method can effectively resist common geometric, filtering, and noise attacks. In conclusion, the frequency-domain watermarking algorithm has greater concealment and robustness than the spatial-domain watermarking algorithm, and DWT in particular has a comprehensive theoretical basis for resilience, which has attracted considerable interest and application in the watermarking design of remote sensing images. However, in the aforementioned studies, it is common to work directly on the RGB color space, which has a certain impact on the chromaticity of the image. In addition, most studies focus on robustness and less on imperceptibility. Therefore, related studies are generally restricted in terms of generality and practicality.

To address the above problems, this study converts remote sensing images from the RGB to YCbCr color space, intends to apply DWT for embedding domain mining of luminance component, selects the most suitable location for watermark embedding combined with the maximum entropy, and adopts the  $\alpha$ -blending method with high-capacity characteristics to accomplish watermark embedding. The ultimate goal of this research is to offer an adaptive watermarking scheme for remote sensing images by combining the aforementioned methods in order to strike a compromise between robustness and invisibility.

## 2. Methodology

### 2.1 Discrete wavelet transform in YCbCr color space

Because each color channel in a color remote sensing image with three or more bands is not independent, the stronger the correlation between them, the more they affect each other. For invisible watermarking to work well, there shouldn't be much difference between the original remote sensing image and the watermarked image. This means that embedding the watermark in one color channel shouldn't have much of an effect on the other color channels. Taking a three-band RGB color remote sensing image as an example, the three channels  $R$ ,  $G$  and  $B$  determine the primary color intensity to produce colors according to the proportion. The RGB color space of an image integrates luminance and chrominance closely, and the embedding of watermarks by modifying the grayscale values of the  $R$ ,  $G$ ,  $B$  and other color channels can readily result in color alterations, thereby reducing the accuracy of the extraction results of ground elements from watermarked remote sensing images. Color is dissected into its luminance ( $Y$ ) and chrominance ( $Cb$  and  $Cr$ ) components inside the YCbCr color space. There isn't much of a relationship between luminance and chrominance, therefore adjusting the brightness may have little effect on the color [25, 26]. When colors are converted to the YCbCr color space, the most energy is concentrated in the  $Y$  channel, which means the  $Y$  channel has the highest entropy value. The human eye is less sensitive to the regions with high entropy, so embedding a watermark in high entropy block can improve its imperceptibility. Also, the

compression and noise overlay used in remote sensing photos have less of an impact on the brightness component. In light of the algorithm's robustness and invisibility, we decided to use the  $Y$  component as the watermark embedding domain. The proposed approach can only be used on multi-band remote sensing images that include the  $R$ ,  $G$  and  $B$  bands and not on the single-band remote sensing images. The equation for converting RGB to YCbCr color space is as follows:

$$\begin{bmatrix} Y \\ Cb \\ Cr \end{bmatrix} = \begin{bmatrix} 0.29900 & 0.58700 & 0.11400 \\ -0.16874 & -0.33126 & 0.50000 \\ 0.50000 & -0.41869 & -0.08131 \end{bmatrix} \begin{bmatrix} R \\ G \\ B \end{bmatrix} \quad (1)$$

where the letters  $R$ ,  $G$  and  $B$  stand for the red, green and blue channels, respectively.  $Y$  indicates luminance, while  $Cb$  and  $Cr$  denote blueness and redness, respectively.

After obtaining the  $Y$  components of the remote sensing image, it is decomposed into two layers using DWT, as depicted in Fig. 1. Using a given filter function, DWT decomposes the luminance  $Y$  into four sub-bands:  $LL_1^Y$  (low frequency),  $LH_1^Y$  (high frequency horizontal component),  $HL_1^Y$  (high frequency vertical component) and  $HH_1^Y$  (high frequency diagonal component). The majority of the signal's energy is located in the low-frequency, while information is sent in the higher-frequency. The original input signal may be recovered quite well by merging the high frequency with the low frequency. In Fig. 1, ' $\downarrow 2$ ' denotes down sampling filter, if  $x[n]$  is used as input, the output is  $y[n] = x[2n]$ .

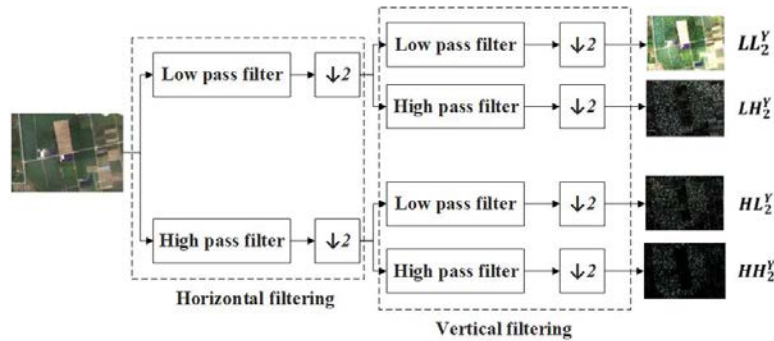


Fig. 1. Two-level DWT on remote sensing images.

The coefficients  $LL_2^Y$ ,  $LH_2^Y$ ,  $HL_2^Y$  and  $HH_2^Y$  can be obtained by repeating DWT on the lower frequency sub-band  $LL_1^Y$  of the original signal. In this study, the input signal is processed using the Haar filter, and the DWT equation is as follows:

$$\begin{cases} LL_2^Y(x, y) = \frac{Y_p(x, y) + Y_p(x, y+1) + Y_p(x+1, y) + Y_p(x+1, y+1)}{2} \\ LH_2^Y(x, y) = \frac{Y_p(x, y) + Y_p(x, y+1) - Y_p(x+1, y) - Y_p(x+1, y+1)}{2} \\ HL_2^Y(x, y) = \frac{Y_p(x, y) - Y_p(x, y+1) + Y_p(x+1, y) - Y_p(x+1, y+1)}{2} \\ HH_2^Y(x, y) = \frac{Y_p(x, y) - Y_p(x, y+1) - Y_p(x+1, y) + Y_p(x+1, y+1)}{2} \end{cases} \quad (2)$$

where  $x$  and  $y$  denote the  $x$  coordinates and  $y$  coordinates of remote sensing image pixels, respectively.  $LL_2^Y$ ,  $LH_2^Y$ ,  $HL_2^Y$  and  $HH_2^Y$  denote the low frequency, high frequency horizontal,

high frequency vertical and high frequency diagonal, which are obtained after DWT transformation of the component, and  $Y_p$  denotes the pixel points of the component  $Y$ .

The sub-band of low-frequency generated by DWT on the component contains the majority of the luminance  $Y$ 's energy. Since embedding watermark information in the low-frequency is likely to cause greater interference with the accuracy of remote sensing images, the high-frequency of the  $Y$  component is selected.

## 2.2 Maximum entropy based embedding location selection

In order to balance the efficiency of watermark embedding with the robustness of the algorithm, this study applies  $8 \times 8$  blocking to the  $HH_2^Y$  band following the DWT transformation of the  $Y$  component. Each sub-block's entropy is then determined, and the sub-block with the greatest entropy is selected as the watermark embedding point. More complex regions of information in an image make it harder for the human eye to detect subtle changes, increasing the watermark's chances of going undetected if placed there. [27]. Typically, entropy is generally used to describe the degree of uncertainty in the occurrence of each possible event of an information source. This study uses entropy to reflect the quantity of average information in the sub-blocks of remote sensing images. Entropy is defined as follows [28]:

$$E = - \sum_{i=1}^N p_i \log_2 p_i \quad (3)$$

where  $p_i$  denotes the probability of occurrence of event  $i$ ,  $0 \leq p_i \leq 1$ , and  $\sum_{i=1}^n p_i = 1$ . The larger  $E$  is, the more complex the image's information, and the sub-block with the highest entropy value is chosen as the watermark embedding domain in this study.

## 2.3 Watermark embedding method based on $\alpha$ -blending

$\alpha$ -blending is a method of mixing pixel color values and producing a transparent effect, which mixes watermark information with the original image to achieve strong concealment for image protection and authentication [29]. As the essence of watermark embedding is to embed transparent or translucent text or images into the original remote sensing image,  $\alpha$ -blending can provide a larger embedding capacity than some traditional watermark embedding methods, allowing more information to be embedded without affecting the image quality or revealing the image source. In addition, the  $\alpha$ -blending method is more resistant to some common image processing operations (e.g. cropping, scaling, rotation, filtering, etc.). In this paper, after converting the watermark image into grayscale, a two-level DWT is done to the grayscale watermark image, and the diagonal component of the watermark is embedded into the block with the highest entropy value of the diagonal component of the remote sense image by  $\alpha$ -blending. The specific equation is as follows:

$$IW_m = (1 - \alpha) \times HH_2^W + \alpha \times block_{max} \quad (4)$$

where  $IW_m$  is the block of the image containing the watermark,  $HH_2^W$  is the diagonal component of the watermark image,  $block_{max}$  is the block with the largest entropy value among the  $8 \times 8$  non-overlapping blocks after applying DWT to the  $Y$  components in the original remote sensing image, and  $\alpha$  is the intensity of the watermark embedding, where  $0 \leq \alpha \leq 1$ . Correspondingly, the extraction equation for the watermarked image is:

$$HH_2^W = \frac{IW_m - \alpha \times block_{max}}{1 - \alpha} \quad (5)$$

### 3. Incorporating and Identifying Watermarks

#### 3.1 The Steps Involved in Adding a Watermark

**Fig. 2** depicts the proposed watermark embedding process, with the following phases of the algorithm:

*Step 1:* Convert the original color remote sensing image from the RGB color space to YCbCr color space to obtain the luminance  $Y$ , chromaticity  $Cb$  and  $Cr$ . Perform the two-level DWT on the luminance component  $Y$  to obtain the high frequency coefficients  $LH_2^Y, HL_2^Y, HH_2^Y$  and the low frequency coefficient  $LL_2^Y$ .

*Step 2:* Divide  $HH_2^Y$  into  $8 \times 8$  non-overlapping blocks and calculate the entropy of each block, where the block with the largest entropy value is referred to as  $block_{max}$ , and its index value  $m$ .

*Step 3:* Applying two-level DWT to a grayscale watermark image  $W$  yields the high frequency coefficients  $LH_2^W, HL_2^W, HH_2^W$ , and the low-frequency coefficient  $LL_2^W$ .

*Step 4:* Embed  $HH_2^W$  into the  $block_{max}$  by  $\alpha$ -blending to obtain the watermarked image blocks  $IW_m$ . The blocks are rearranged according to the original order of  $HH_2^Y$  and merged to form  $(HH_2^Y)'$ .

*Step 5:* Perform inverse DWT on  $LH_2^Y, HL_2^Y, LL_2^Y$  and  $(HH_2^Y)'$  using the following equation to obtain the new luminance  $Y_{new}$ :

$$Y_{new} = IDWT[LL_2^Y, HL_2^Y, LH_2^Y, (HH_2^Y)'] \quad (6)$$

*Step 6:* Combining  $Cb, Cr$  and  $Y_{new}$  yields the watermarked remote sensing image. Finally, the watermarked remote sensing image  $IW$  is generated by transforming the image from YCbCr to RGB.

After the watermark has been embedded, the peak signal-to-noise ratio (PSNR) and structural similarity (SSIM) are calculated to determine the fidelity of the watermarked images and the imperceptibility of the watermarking, which is calculated as [30]:

$$PSNR = 10 \times \log_{10} \frac{(M \times N) \times [\max(I) - \min(I)]^2}{\sum_{i=1}^M \sum_{j=1}^N [I(i,j) - I'(i,j)]^2} \quad (7)$$

where  $I$  and  $I'$  denote the host image and watermarked image, respectively.  $I(i,j)$  and  $I'(i,j)$  are the image element values corresponding to the host and watermarked images. SSIM is designed to work like the human visual system by emphasizing features like edge and texture similarity, its specific equation is as follows:

$$SSIM(x, y) = \frac{(2\mu_x\mu_y)(2\sigma_{xy}+C_2)}{(\mu_x^2+\mu_y^2+C_1)(\sigma_x^2+(\sigma_y^2+C_2)} \quad (8)$$

where  $\mu_x$  is the average value of  $x$ ,  $\mu_y$  is the mean of  $y$ ,  $\sigma_x^2$  and  $\sigma_y^2$  are the  $x$  and  $y$  variances, respectively, and  $\sigma_{xy}$  is the covariance. The constant  $C_1 = (k_1L)^2$  and  $C_2 = (k_2L)^2$  are the stabilizing constants. When  $k_1 = 0.01$ ,  $k_2 = 0.03$ ,  $L$  represents the range of possible pixel values. Similarity between two images is measured using the SSIM scale, which runs from 0 to 1.

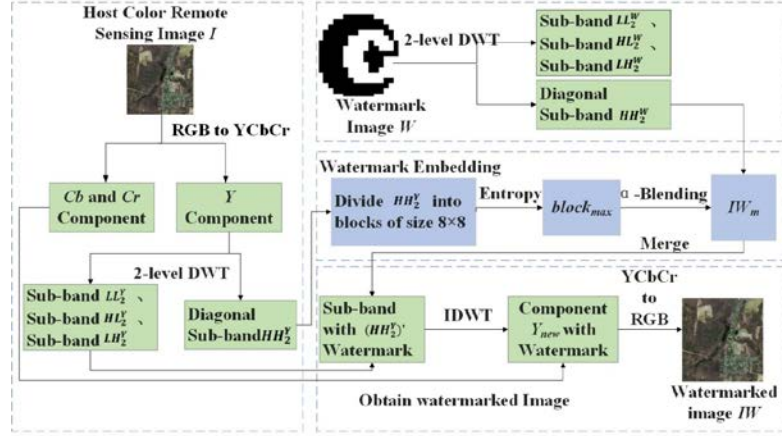


Fig. 2. Watermark embedding process.

### 3.2 Process of Watermark Extraction

Watermark extraction is the technique of extracting the watermark embedded in the protected data. The watermark extraction is displayed in Fig. 3, and its individual stages are as follows:

*Step 1:* Convert the watermarked image  $IW$  from the RGB to YCbCr color space to obtain the luminance  $Y_{new}$ , chromaticity  $Cb$  and  $Cr$ . Perform the two-level DWT on the luminance component  $Y_{new}$  to obtain the high-frequency coefficient  $(HH_2^Y)'$ .

*Step 2:* Separate  $(HH_2^Y)'$  into  $8 \times 8$  blocks, choose  $IW_{blocks}$  blocks with the maximum entropy as the  $block_{max}$  containing the watermark, the index of this block is recorded as  $m$ .

*Step 3:* The diagonal component  $(HH_2^W)'$  of the watermark is obtained by performing the inverse  $\alpha$ -blending operation.

*Step 4:* Perform inverse DWT on the  $LH_2^W$ ,  $HL_2^W$ ,  $LL_2^W$  and  $(HH_2^W)'$  to obtain the watermark image  $W'$ .

*Step 5:* Before extraction, the image is subjected to various attacks, including noise, JPEG compression, cropping, median filtering, and various geometric attacks, to evaluate the robustness of the proposed scheme. NC is used to analyze the robustness of the watermarking scheme by calculating the degree of similarity between the extracted and original watermarks, which is given by [30]:

$$NC = \frac{\sum_{i=1}^m \sum_{j=1}^n W'(i,j)W(i,j)}{\sum_{i=1}^m \sum_{j=1}^n W^2(i,j)} \quad (9)$$

where  $m \times n$  is the watermark size;  $W$  and  $W'$  denote the embedded and extracted watermarks, respectively; and  $W(i,j)$  and  $W'(i,j)$  are the pixel values of the embedded and extracted watermark at the  $(i,j)$ .

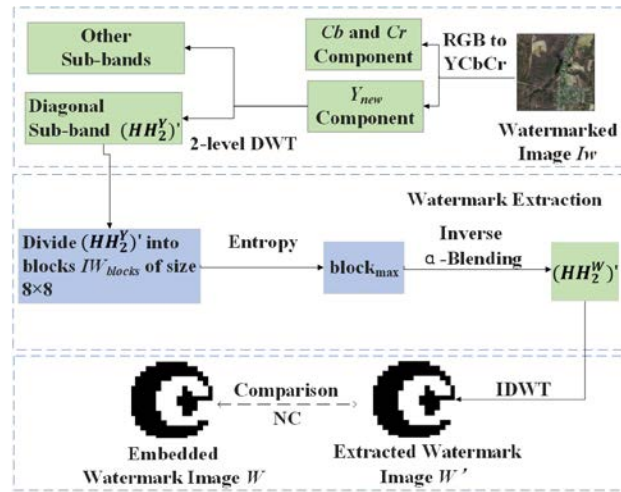


Fig. 3. Watermark extraction process.

## 4. Experimental Results and Analysis

### 4.1 Experimental data

Six remote sensing images are selected as test data to evaluate the performance of the proposed algorithm. After embedding the watermark, the imperceptibility analysis of the watermarked image is carried out and the watermark information is extracted under a variety of attacks to test the algorithm's robustness. The remote sensing images used for testing are shown in Fig. 4, where (a) is public data from Sentinel-2, (b) and (d) is public data downloaded from Google Earth, (c) is public data from Massachusetts, (e) is public data from WorldView-3, and (f) is UAV data. Table 1 details the data in full depth. The watermark image is a binary image of size  $16 \times 16$ , as shown in Fig. 5.

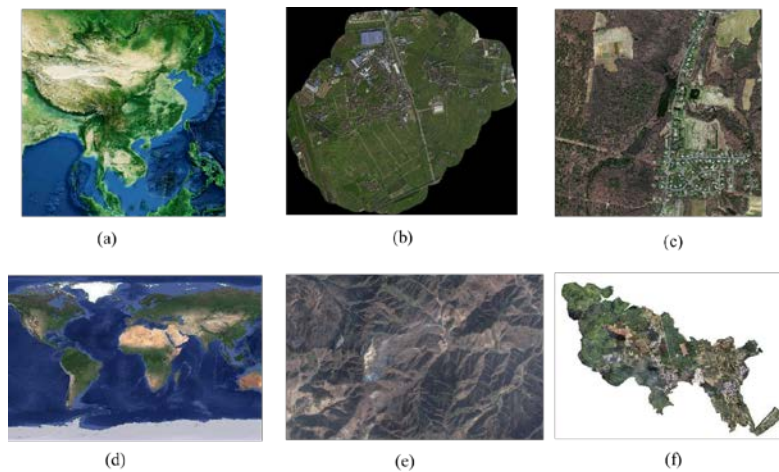


Fig. 4. Experimental data sets.



**Table 1.** Details of test remote sensing images

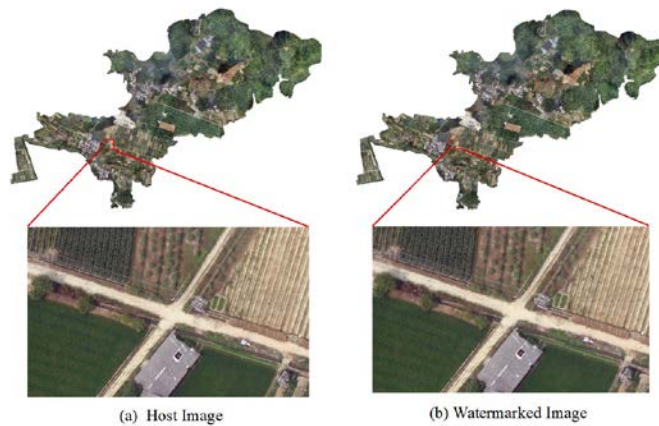
Data sets	Resolution	Image size	Source
(a)	500m	1456*1456	Sentinel-2
(b)	0.8 m	3185*3185	Google Earth data
(c)	1 m	1500*1500	Massachusetts data
(d)	78046m	256*512	Google Earth data
(e)	96m	8608*4528	WorldView-3
(f)	0.1 m	1180*1180	UAV data

**Fig. 5.** Watermark image.

## 4.2 Imperceptibility Analysis

**Fig. 6** displays a side-by-side comparison of the original remote sensing image and the watermarked version, with the watermark embedding strength  $\alpha$  set to 0.35. It is difficult to visually distinguish the difference between them based on the macroscopic display and detailed comparison, implying that there is no noticeable degradation in image quality as a result of watermark embedding.

The proposed algorithm's efficiency is measured against existing methods in the literature [21] and [31], which are relatively recent and similar to this paper in terms of the underlying algorithm, in order to evaluate its performance. Watermarked remote sensing image PSNR and SSIM under this paper's algorithm and the compared algorithms are shown in **Table 2**. The proposed watermarking yields post-encoding PSNR values greater than 50, whereas the PSNR values of [21] are all less than 29 and those of the literature [31] are all less than 34. The SSIM values of the watermarked images under the proposed algorithm are all higher than 0.9970, while the SSIM values of [21] are all less than 0.91, and most of the SSIM values of [31] are also lower than the proposed algorithm. Combining visual observation and quantitative analysis, the proposed watermarking algorithm has excellent invisibility.

**Fig. 6.** Comparison of remote sensing images before and after watermark embedding.

**Table 2.** Invisibility comparison

Evaluation indicators	Data sets	The proposed scheme	[21]	[31]
PSNR	(a)	48.6818	26.3464	47.2036
	(b)	51.07	28.27	33.0300
	(c)	50.6	26.10	33.0300
	(d)	46.6800	28.8981	47.5264
	(e)	46.9086	28.6704	35.3423
	(f)	52.52	28.96	33.04
SSIM	(a)	0.9985	0.8561	0.9979
	(b)	0.9970	0.8988	0.9952
	(c)	0.9981	0.8549	0.9982
	(d)	0.9970	0.8973	0.9970
	(e)	0.9976	0.8243	0.9974
	(f)	0.9976	0.9094	0.9845







### 4.3 Analysis of robustness



















Remote sensing images are subject to various forms of attacks in the process of acquisition, transmission and application, causing problems such as image corruption and quality degradation. The ability to successfully extract watermark data and verify copyright under varying attack modes is crucial for data protection. This study compares the magnitude of NC values to evaluate the similarity between the original watermark and the extracted watermarks to validate the algorithm's robustness against varying attacks. Due to page length constraints, each attack experiment presents the results in a set of data, and the effect is approximately the same for other data.

#### 4.3.1 Resistant to Geometric Attacks

The most frequent kinds of geometric assaults include rotations, scaling, and translations. In this study, we perform a variety of geometric attacks on watermarked remote sensing images. **Table 3** displays the comparison between this paper's proposed algorithm and the ones presented in [21] and [31]. The results show that the NC values for the proposed watermarking are more than 0.97, and the extracted watermark images are clear with basically no cluttered points, even when subjected to various degrees of rotation and scaling attacks. The watermark images extracted by the algorithm described in [21] can also be identified, but most of the NC values are less than 0.91, and there are some noise points that will hinder copyright recognition. The algorithm described in [31] is resistant to scaling attacks, but not rotation or translation attacks, and cannot extract a watermark image that is recognizable. The proposed watermarking is shown to be highly resistant to common geometric attacks.

**Table 3.** Results of RST attacks

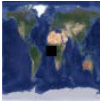



















Attack mode	Scale	The proposed scheme	[21]	[31]
Rotation	1°	 NC=0.9742	 NC=0.8910	 NC=0.9175
	10°	 NC=0.9709	 NC=0.9025	 NC=0.4936

	75°	 NC=0.9708	 NC=0.8779	 NC=0.6515
Scaling	0.5 time	 NC=0.9703	 C=0.9065N	 NC=0.9834
	2 time	 NC=0.9703	 NC=0.9065	 NC=0.9864
Translation	Translate 100 to the right	 NC=0.9679	 NC=0.9065	 NC=0.1038
	Translate 100 to the bottom	 NC=0.9708	 NC=0.9065	 NC=0.0694
	Translate 100 to the bottom right	 NC=0.9745	 NC=0.9065	 NC=0.0497

### 4.3.2 Resistant to Cropping Attacks

Cropping is a widely used data editing method in remote sensing images because it allows users to quickly and effectively isolate the required target region or feature pieces from an otherwise unmanageable data set. [Table 4](#) details the results of a series of cropping attacks performed on experimental data to verify that the proposed watermarking is robust against such assaults. In spite of an increase in the cropping area, the findings show that the proposed watermarking is able to accurately extract watermark information. For example, when the area is cropped by 1/2, the NC value can still reach 0.9735. The algorithm in [\[21\]](#) can resist attacks with different cropping areas, but the integrity of the extracted watermark is low and the NC values are lower than the proposed algorithm. The algorithm in [\[31\]](#) fails to extract watermark information when cropping small areas and performs even worse at larger scales, exhibiting little resistance to crop attacks. The main reason is that irregular cropping attacks will affect the embedding position of the watermark, resulting in an extraction that is incomplete. The algorithm presented in [\[31\]](#) cannot achieve adaptive embedding of the watermark because it relies on the watermark's integrity; therefore, the extraction of the watermark fails. Whereas the algorithm in this paper adaptively selects the embedding position of the watermark according to the features of the remote sensing images, and embedding the watermark information in the key position of the image, so ensuring the robustness against cropping attacks.

**Table 4.** Results of cropping attacks

Cropping scale	Attack mode	The proposed scheme	[21]	[31]
Center attack		 NC=0.9693	 NC=0.8944	 NC=0.98522
Cut 1/4 on top left corner		 NC=0.9729	 NC=0.8812	 NC=0.7626
Cut 1/4 on bottom right corner		 NC=0.9712	 NC=0.9380	 NC=0.8420
Cut 1/2 on the left		 NC=0.9737	 NC=0.9380	 NC=0.8405
Cut 1/2 on the top		 NC=0.9735	 NC=0.9305	 NC=0.7970

### 4.3.3 Resistant to Filtering Attacks

Filtering is a common operation encountered in the interpretation of remote sensing images. In this paper, data (b) is used to test Gaussian filtering attack, data (a) is used to test mean filtering attacks, and data (e) is used to test Wiener filtering attacks. The watermarked remote sensing images are filtered with varying degrees of Gaussian low-pass, mean, and Wiener filtering, and the NC values of the extracted watermark images are counted to demonstrate the practicality of the proposed watermarking; the results are depicted in [Fig. 7](#), [Fig. 8](#) and [Fig. 9](#).

Under the Gaussian low-pass filtering attacks, when the attack intensity is  $1 \times 1$ , the NC value of the watermark extracted by the algorithm in this paper is 1, indicating that the watermark can be extracted in its entirety. Under the attack intensities of  $2 \times 2$ ,  $3 \times 3$  and  $4 \times 4$ , the proposed watermarking is more resistant than the algorithm presented in the [\[31\]](#), and the NC values are greater than 0.96, whereas the extracted watermark integrity in [\[21\]](#) is low. Even when the attack intensity reaches  $9 \times 9$ , the proposed algorithm can successfully extract watermark information accurately, and the NC value can still reach 0.9704, while the algorithms in the comparison papers cannot extract the watermark completely, and their NC values are all less than 0.91. Gaussian low-pass filtering will smooth the high-frequency detail information of the remote sensing images, weakening or eliminating the high-frequency components used in the watermark embedding, the proposed algorithm uses DWT to divide blocks, and discrete wavelets can decompose the signal at different scales, reducing the interference of Gaussian low-pass filtering on watermark extraction, thus enhancing the watermarking resistance.

Mean filtering employs the same attack strength as Gaussian low-pass filtering, and when the attack strength is  $1 \times 1$ , the NC value extracted by the proposed algorithm is 1. For weaker watermark attacks, such as  $2 \times 2$  and  $3 \times 3$ , the extraction results of the proposed algorithm and the algorithm presented in [\[31\]](#) are superior. However, the algorithms in the comparative literature are incapable of extracting accurate watermark information under high-intensity attacks, while the proposed algorithm maintains a high level of robustness. The results show that the proposed watermarking algorithm is likewise highly robust to the mean filtering attack.

The Wiener filtering attack will smooth the image and blur the information of the image's high frequency details, thereby affecting the extraction of the watermark. The NC values of the extracted watermark images from the proposed algorithm are greater than 0.97 under varying strengths of Wiener filtering attacks, demonstrating once again its extremely robust nature. The algorithm in [21] is resistant to Wiener filtering attacks, it can't compare to the proposed algorithm in terms of watermark extraction integrity, and the NC values are all close to 0.94; the algorithm in [31] is not resistant to Wiener filtering attacks and cannot extract the complete watermark information.

This paper's DWT incorporates elements from both the time domain and the frequency domain, making it resistant to filtering attacks that target high-frequency information. The experimental outcomes prove the filtering-attack-resistance of the proposed watermarking algorithm.

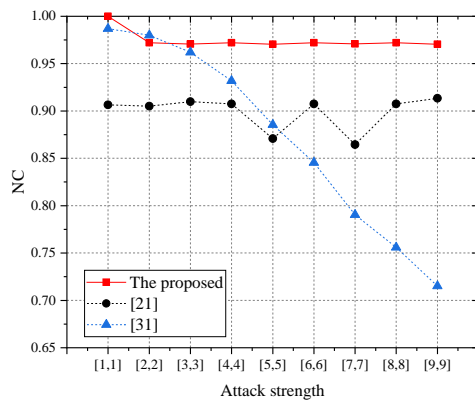


Fig. 7. Results of Gaussian filtering attacks.

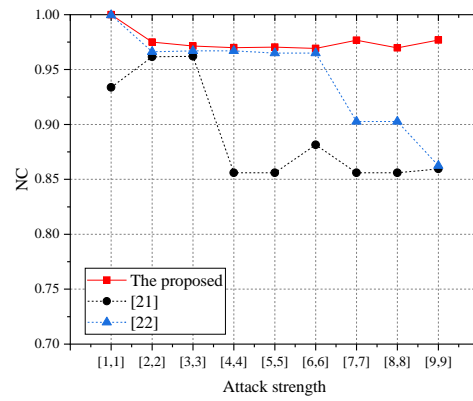


Fig. 8. Results of mean filtering attacks.

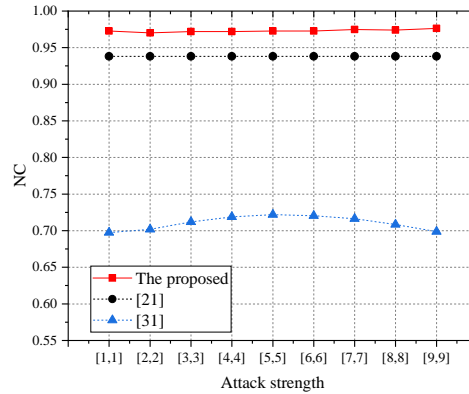


Fig. 9. Results of Wiener filtering attacks.

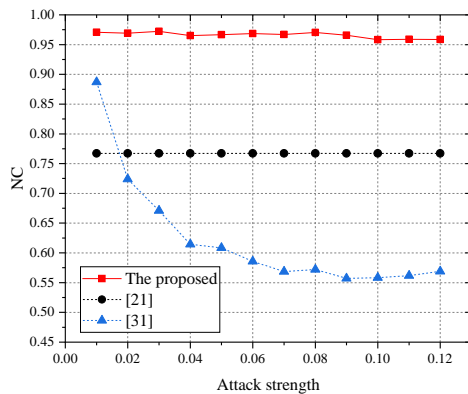
#### 4.3.4 Resistant to Noise Attacks

Noise is very simple to generate during remote sensing image processing, therefore, robustness against noise attacks is an essential property of watermarking algorithms. Experiments in this section employ three distinct noise attacks: pepper noise, scattered noise, and Gaussian noise. Fig. 10, Fig. 11, and Fig. 12 depict the watermark extraction results of the proposed algorithm and the comparative paper algorithms under the three noise attacks. In this paper, data (e) is used to test Pepper noise attack, data (b) is used to test Scattered noise attacks, and data (a) is used to test Gaussian noise attacks.

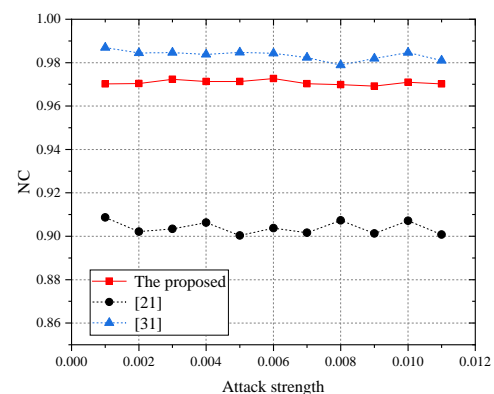
When the pepper noise attack intensity is less than 0.06, the NC values extracted by the proposed algorithm are higher than 0.96. Under different intensities of pepper noise attacks, the NC values of the watermark extracted by the algorithm from [21] are 0.7671, which is lower than the proposed algorithm. While the NC value of the watermark information extracted by the algorithm in [31] is less than 0.7 due to the increase of random black and white pixels introduced by the pepper noise under high attack intensity. With the gradual increase of attack intensity, the watermark integrity extracted by the proposed algorithm tends to decrease gradually; however, the NC values are all greater than 0.958, and the extracted watermarks' integrity has a very obvious advantage over the comparison literature.

Under varying intensities of scattering noise attacks, the mean NC of the extracted watermarks from the proposed watermarking scheme is higher than 0.97, which is slightly lower than the results of the paper [31], but still has a good ability to resist scattering noise attacks. As scattering noise is caused by the interference of light, which leads to random light and dark changes in remote sensing images, the proposed algorithm performs watermark embedding on the basis of the frequency domain and is able to reduce the influence of scattering noise through frequency domain transformation.

The proposed algorithm, along with that of the paper [21], performs better under varying degrees of Gaussian noise attacks, and its NC values are also slightly higher than those of the paper [21]. In contrast, the algorithm in the paper [31] is completely vulnerable to Gaussian noise. Gaussian noise is a type of random noise resulting from electronic noise generated during the image acquisition process or interference in signal transmission, etc. Increases in attack strength have a multiplicative effect on watermark interference during extraction, which in turn alters the watermark's embedding position. The proposed algorithm combines DWT and maximum entropy with frequency domain space and adaptive embedding to improve the algorithm's robustness against noise interference on the watermark. In summary, the proposed algorithm is very robust against noise attacks, and its performance is very stable and less affected by changes in attack scale.



**Fig. 10.** Results of Pepper noise attacks.



**Fig. 11.** Results of Scattered noise attacks.

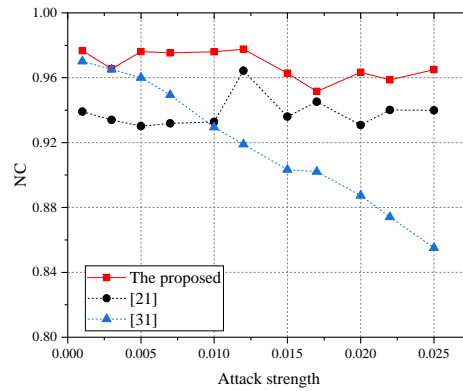









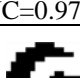
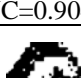
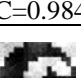
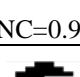
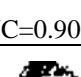
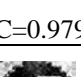


Fig. 12. Results of Gaussian noise attacks.

#### 4.3.5 Resistant to Compression Attacks

Compression of remote sensing images is a common pre-processing operation in the data processing, storage, and transmission workflow. Table 5 displays the specific attack scales used in these tests and the resulting watermark detection rates for the watermarked remote sensing images. According to the statistical results, the extracted watermarks' NC values are all higher than 0.9708 under compression with varying quality factors, and the extracted watermarks are distinct and recognizable. The NC values obtained from the algorithm in [21] are all less than 0.91, and there are more noise points. Although the algorithm in [31] has good robustness to attack for some of the factors in JPEG compression, the robustness to attack is unstable and even some of the results are challenging to recognize. The proposed algorithm demonstrates very stable robustness against JPEG compression attacks with varying quality factors and can effectively resist JPEG compression attacks.

Table 5. Results of JPEG compression attacks

Attack	Quality Factors	The proposed scheme	[21]	[31]
JPEG Compression	90	 NC=0.9724	 NC=0.9058	 NC=0.9860
	70	 NC=0.9708	 NC=0.9039	 NC=0.8723
	50	 NC=0.9729	 NC=0.9047	 NC=0.9847
	30	 NC=0.9708	 NC=0.9034	 NC=0.9797
	10	 NC=0.9708	 NC=0.8464	 NC=0.9537

## 5. Conclusion

This study applies DWT and the entropy method to YCbCr color space to develop an adaptive watermarking scheme for remote sensing images. The algorithm performs a two-level DWT transform on the luminance component and improves the watermark embedding efficiency and robustness by means of blocking. On this basis, the entropy value of each sub-block is calculated, the sub-block with the high energy is chosen as the watermark embedding location, where the watermark is embedded by means of  $\alpha$ -blending. Through detailed comparison and quantitative analysis of the remote sensing images after embedding the watermark, it has been determined that the watermark embedding has a negligible effect impact on the quality of the data, and the advantage in terms of invisibility is readily apparent when compared to the comparative literature. In terms of robustness, it has excellent performance in geometric attacks, filtering attacks, noise attacks, and compression, and it is very stable, not easily changing in response to changes in the intensity of the attacks, demonstrating extremely superior robustness. The proposed algorithm has excellent integrity and stability, mainly in that the block with maximum entropy maintains the same position under different degrees and types of attacks, allowing us to always find the correct watermark embedding domain, which is also one of the important reasons for the robustness of the proposed algorithm.

The proposed watermarking provides reliable support for the comprehensive performance improvement of the algorithm in the details of blocking, frequency domain selection and intensity setting, and the adaptive approach strikes a good balance between the algorithm's invisibility and robustness. The research can serve as a technical reference for the security protection of multi-band remote sensing images, but it is inapplicable to single-band remote sensing image data. Subsequent research will expand the algorithm's applicability to a wider range of scenarios.

## References

- [1] H. Ghassemian, "A review of remote sensing image fusion methods," *Information Fusion*, vol. 32, pp. 75-89, 2016. [Article \(CrossRef Link\)](#)
- [2] G. Cheng, J. Han, and X. Lu, "Remote sensing image scene classification: Benchmark and state of the art," *Proceedings of the IEEE*, vol. 105, no. 10, pp. 1865-1883, 2017. [Article \(CrossRef Link\)](#)
- [3] X. Wang, J. Huang, Y. Chu, A. Shi and L. Xu, "Change Detection in Bitemporal Remote Sensing Images by using Feature Fusion and Fuzzy C-Means," *KSII Transactions on Internet and Information Systems*, vol. 12, no. 4, pp. 1714-1729, 2018. [Article \(CrossRef Link\)](#)
- [4] D. Li, L. Zhang, and G. Xia, "Automatic analysis and mining of remote sensing big data," *Acta Geodaetica et Cartographica Sinica*, vol. 43, no. 12, pp.1211-1216, 2014. [Article \(CrossRef Link\)](#)
- [5] A.M. Lechner, G.M. Foody, D.S. Boyd, "Applications in remote sensing to forest ecology and management," *One Earth*, vol. 2, no. 5, pp. 405-412, 2020. [Article \(CrossRef Link\)](#)
- [6] B. Carpentieri, A. Castiglione, A.D. Santis, F. Palmieri and R. Pizzolante, "One-pass lossless data hiding and compression of remote sensing data," *Future generation computer systems*, vol. 90, pp. 222-239, Jan. 2019. [Article \(CrossRef Link\)](#)
- [7] X. Xi, Y. Hua, Y. Chen and Q. Zhu, "Zero-watermarking for vector maps combining spatial and frequency domain based on constrained Delaunay triangulation network and discrete Fourier transform," *Entropy*, vol. 25, pp. 682, 2023. [Article \(CrossRef Link\)](#)
- [8] C. Zhu, N. Ren and D. Xu, "Geo-information security technology: progress and prospects," *Acta Geodaetica et Cartographica Sinica*, vol. 51, no. 6, pp. 1017-1028, 2022. [Article \(CrossRef Link\)](#)
- [9] C. I. Podilchuk, W. Zeng, "Image-adaptive watermarking using visual models," *IEEE Journal on Selected Areas in Communications*, vol. 16, no. 4, pp. 525-539, May. 1998. [Article \(CrossRef Link\)](#)



- [10] G. Hua, J. Huang, Y.Q. Shi, J. Goh, V.L.L. Thing, "Twenty years of digital audio watermarking - a comprehensive review," *Signal Processing*, vol. 128, pp. 222-242, 2016. [Article \(CrossRef Link\)](#)
- [11] M. Asikuzzaman, M.R. Pickering, "An overview of digital video watermarking," *IEEE Transactions on Circuits and Systems for Video Technology*, vol. 28, no. 9, pp. 2131-2153, 2018. [Article \(CrossRef Link\)](#)
- [12] M.H. Alkawaz, G. Sulong, T. Saba, A.S. Almazayad and A. Rehman, "Concise analysis of current text automation and watermarking approaches," *Security and Communication Networks*, vol. 9, pp. 6365-6378, 2016. [Article \(CrossRef Link\)](#)
- [13] X. Xu, X. Zhang, Y. Sun, J. Xin, and Q. Xin, "Topology-Preserving and Geometric Feature-Correction Watermarking of Vector Maps," *IEEE Access*, vol. 8, pp. 33428-33441, 2020. [Article \(CrossRef Link\)](#)
- [14] B.P. Kumari, V.P.S. Rallabandi, "Modified patchwork-based watermarking scheme for satellite imagery," *Signal Processing*, vol. 88, no. 4, pp. 891-904, 2008. [Article \(CrossRef Link\)](#)
- [15] P. Zhu, F. Jia, J. Zhang, "A copyright protection watermarking algorithm for remote sensing image based on binary image watermark," *Optik*, vol. 124, no. 20, pp. 4177-4181, 2013. [Article \(CrossRef Link\)](#)
- [16] M. R. Khosravi, H. Rostami, S. Samadi, "Enhancing the binary watermark-based data hiding scheme using an interpolation-based approach for optical remote sensing images," *International Journal of Agricultural and Environmental Information Systems*, vol. 9, no. 2, pp. 53-71, 2018. [Article \(CrossRef Link\)](#)
- [17] N. Ren, C. Zhu, Z. Wang, "Semi-blind watermarking algorithm resistance on geometrical attacks for high-resolution remote sensing image," *Geomatics and Information Science of Wuhan University*, vol. 36, no.3, pp. 329-332, 2011. [Article \(CrossRef Link\)](#)
- [18] S. B. Ziegeler, H. Tamhankar, J. E. Fowler, L. M. Bruce, "Wavelet-based watermarking of remotely sensed imagery tailored to classification performance," in *Proc. of IEEE Workshop on Advances in Techniques for Analysis of Remotely Sensed Data*, Greenbelt, MD, pp. 259-262, 2003. [Article \(CrossRef Link\)](#)
- [19] N. Agarwal, A.K. Singh, P.K. Singh, "Survey of robust and imperceptible watermarking," *Multimedia Tools and Applications*, vol. 78, pp. 8603-8633, 2019. [Article \(CrossRef Link\)](#)
- [20] D. Tong, N. Ren, C. Zhu, "Secure and robust watermarking algorithm for remote sensing images based on compressive sensing," *Multimedia Tools and Applications*, vol. 78, pp. 16053-16076, 2019. [Article \(CrossRef Link\)](#)
- [21] G. Yuan, Q. Hao, "Digital watermarking secure scheme for remote sensing image protection," *China communications*, vol. 17, no. 4, pp. 88-98, 2020. [Article \(CrossRef Link\)](#)
- [22] L. Li, J. Sun, "A watermarking algorithm for remote sensing image based on DFT and watermarking segmentation," *Advanced Materials Research*, vol. 433-440, pp. 2504-2508, 2012. [Article \(CrossRef Link\)](#)
- [23] D. Li, X. Che, W. Luo, Y. Hu, Y. Wang, Z. Yu, and L. Yuan, "Digital watermarking scheme for color remote sensing image based on quaternion wavelet transform and tensor decomposition," *Mathematical Methods in the Applied Sciences*, vol. 42, no. 14, pp. 4664-4678, 2019. [Article \(CrossRef Link\)](#)
- [24] R. Qin, L. Zhang, T. Wu, Y. Li, H. Wang, "A blind watermarking algorithm for remote sensing image based on anti-affine transformation combining ASIFT and normalization," *Journal of Geo-Information Science*, vol. 23, no. 10, pp. 1882-1891, 2021.
- [25] S. Kumar, B. K. Singh, "DWT based color image watermarking using maximum entropy," *Multimedia Tools and Applications*, vol. 80, pp. 15487-15510, 2021. [Article \(CrossRef Link\)](#)
- [26] T. Zhu, H. Cao, Y. Liu, P. Bi, "Dual watermarking algorithm for color image based on improved color space," *Control and Decision*, vol. 34, pp. 1141-1150, 2019.
- [27] J. Serra-Ruiz, A. Qureshi, D. Megías, "Entropy-based semi-fragile watermarking of remote sensing images in the wavelet domain," *Entropy*, vol. 9, pp. 847, 2019. [Article \(CrossRef Link\)](#)
- [28] Y. Gangadhar, A. V. S. Giridhar, R. P. Chenna, "An evolutionary programming approach for securing medical images using watermarking scheme in invariant discrete wavelet transformation," *Biomedical Signal Processing and Control*, vol. 43, pp. 31-40, 2018. [Article \(CrossRef Link\)](#)

- [29] E. Fragoso-Navarro, M. Cedillo-Hernández, M. Nakano-Miyatake, A. Cedillo-Hernández, and H.M. Pérez-Meana, “Visible watermarking assessment metrics based on just noticeable distortion,” *IEEE Access*, vol. 6, pp. 75767-75788, 2018. [Article \(CrossRef Link\)](#)
- [30] T. Qing, B. Chen, “Robust color image watermarking technique in the spatial domain,” *Soft Computing*, vol. 22, pp. 91–106, 2018. [Article \(CrossRef Link\)](#)
- [31] J. Liu, J. Huang, Y. Luo, L. Cao, S. Yang, D. Wei, and R. Zhou, “An optimized image watermarking method based on HD and SVD in DWT domain,” *IEEE Access*, vol. 7, pp. 80849-80860, 2019. [Article \(CrossRef Link\)](#)



**Yang Hua** is a senior majoring in Geographic Information Science at Suzhou University of Science and Technology. Her research interests include information security, watermarking for geo-spatial data and blockchain.



**Xu Xi** received the B.S. degree from Zhengzhou University, Zhengzhou, China, in 2012, the M.S. degree from Liaoning Normal University, Dalian, China, in 2015, and the Ph.D. degree from Sun Yat-sen University, Guangzhou, China, in 2020. He is currently an associate professor with the School of Geography Science and Geomatics Engineering, Suzhou University of Science and Technology. His research interests include geospatial data security, digital watermarking, and GIS application and analysis.



**Chengyi Qu** received the B.S. degree from NanJing XiaoZhuang University, Nanjing, China, in 2019. He is currently purchasing M.S. degree at Suzhou University of Science and Technology, Suzhou, China. Before entering Suzhou University of Science and Technology, he was a R&D Engineer of Piesat Information Technology Co., Ltd during 2019 to 2021. His research interests include geospatial data security and digital watermarking.



**Jinglong Du** received the B.S., M.S., and Ph.D. degrees from East China Normal University, Shanghai, China, in 1992, 2002, and 2006, respectively. He is currently a Professor with the School of Geography Science and Geomatics Engineering, Suzhou University of Science and Technology. He is a member of China geographic information society and the director of the big data research center of Suzhou Institute of urban and rural integration reform and development. His research interests include geospatial data security, intelligent environmental protection and GIS application and analysis.



**Maofeng Weng** received the B.S. degree from Zhengzhou University, Zhengzhou, China, in 2012. He is currently a registered engineer of civil engineering with the Northwest Engineering Corporation Limited, PowerChina. His main research directions include big data analysis and information security.



**Bao Ye** received the B.S. degree in surveying engineering from Wuhan Technic University of Surveying and Mapping in 1999, and obtained the M.S. degree in surveying and mapping engineering from Tongji University in 2010, a senior engineer and a national registered surveyor. His main research fields include urban three-dimensional datum, precision engineering surveying, spatial data processing, etc.